Available online at www.sciencedirect.com
SCIENCE DIRECT®
Journal of Solid State Chemistry 174 (2003) 52–59
JOURNAL OF SOLID STATE CHEMISTRY
http://elsevier.com/locate/jssc

Correlation between structure and magnetic properties of Cd-substituted $La_{0.7}(Ca_{0.3-x}Cd_x)MnO_3$ CMR manganites

A. Peña,[a,*] J. Gutiérrez,[b] J.M. Barandiarán,[b] J.P. Chapman,[a] M. Insausti,[a] and T. Rojo[a]

[a] *Departamento de Química Inorgánica, Facultad de Ciencias, Universidad del País Vasco/EHU, Apartado 644, E-48080 Bilbao, Spain*
[b] *Departamento de Electricidad y Electrónica, Facultad de Ciencias, Universidad del País Vasco/EHU, Apartado 644, E-48080 Bilbao, Spain*

Received 26 November 2002; received in revised form 11 March 2003; accepted 15 March 2003

Abstract

Structural, electrical and magnetic properties of Cd-doped $La_{0.7}(Ca_{0.3-x}Cd_x)MnO_3$ ($0 \leqslant x \leqslant 0.3$) manganites are presented. All compositions were indexed in the orthorhombic (*Pnma*) space group, except the $Cd_{0.3}$ sample, indexed as a combination of trigonal ($R\bar{3}c$) and orthorhombic (*Pnma*) space groups. Substitution of Ca by Cd has a strong influence on the magnetic and magnetoresistive properties of these compounds, continuously decreasing both the magnetic moment and the Curie temperature (from 3.5 μ_B and 270 K for the $x = 0$ composition to 1.59 μ_B and 90 K for the fully doped $x = 0.3$ one). Samples corresponding to $x = 0$ and 0.1 show a semiconductor–metal transition at temperatures close to the Curie ones. The measured magnetoresistance change is about 49% at 270 K and 95% at 165 K for those samples, respectively. However, the $x = 0.2$ and 0.3 compositions show insulating behaviour in the whole temperature range studied, with values of the magnetoresistance about 85% at 105 K and 74% at 90 K, respectively. The observed weakening of the double-exchange mechanism as the Cd doping level in these samples increases is discussed in terms of structural properties, cationic disorder and Mn^{3+}/Mn^{4+} content ratio.

Keywords: Manganites; Crystal structure; Magnetization; Magnetoresistance; Semiconductor–metallic transition

1. Introduction

Perovskite-like phases with the general formula $Ln^{3+}_{1-x}M^{2+}_xMnO_3$ (Ln^{3+} = La, Pr, Nd, Sm, … and M^{2+} = Ca, Sr, Ba, Pb, …) have attracted the attention of the scientific community due to the magnetotransport properties exhibited [1,2]. The double-exchange mechanism [3] is used to explain the ferromagnetic behaviour of these phases, while the simultaneous presence of ferromagnetism and metallic state brings about magnetoresistance when the magnetic field is changed [4]. The rhombohedral and orthorhombic distortion of the actual crystallographic structure of the classic cubic symmetry is an essential factor to understand the magnetic and transport properties of these samples. Another lattice effect inherent to these compositions is the random disorder of Ln^{3+} and M^{2+} cations with different sizes distributed over the A sites in the ABO_3 perovskite structure. This influence can be quantified by calculating the variance of the cation radius distribution, σ^2, about the mean ionic radii $\langle r_A \rangle$ [5].

Several reports have been published describing Ca^{2+} (ionic radius 1.18 Å) as a divalent doping element [6–8]. The close value of the Cd^{2+} ionic radius (1.15 Å) seems to indicate that direct substitution of Ca ions by Cd ones can be performed without dramatic changes in the structural and magnetic properties. This fact has prompted a search for higher values of the magnetic order temperature (T_C) in several $(La–Ca)MnO_3$ families of compounds [9–12], ferromagnetic character of the sample and the existence of magnetoresistive behaviour. However, the observed magnetic properties differ from the expected ones: in bulk samples, doping with Cd leads to weaker ferromagnetic interactions giving rise to lower T_C values, and strongly favours insulating behaviour [10–12]. The different electronegativities of both compounds, 1 Pauling for Ca ion and 1.69 Pauling for the Cd one [13], must also be taken into account when explaining such behaviour.

In this work, we present the results concerning the magnetic and structural properties of the

*Corresponding author. Fax: +34-94-464-8500.
E-mail address: qippezoa@lg.ehu.es (A. Peña).

0022-4596/03/$ - see front matter © 2003 Elsevier Science (USA). All rights reserved.
doi:10.1016/S0022-4596(03)00173-7

$La_{0.7}Ca_{0.3}MnO_3$ perovskite when Ca^{2+} is substituted progressively by Cd^{2+}. We were especially careful in the analysis of the structural properties of the studied compositions (space group and cationic disorder), and tried to explain the observed magnetic and magneto-transport properties on the basis of the previously determined structural ones.

2. Experimental

Mixed oxides of nominal composition $La_{0.7}(Ca_{0.3-x}Cd_x)MnO_3$ $(0 \leqslant x \leqslant 0.3)$ were prepared by the sol–gel method with the required quantities of analytical grade of La_2O_3, $Ca(NO_3)_2 \cdot 4H_2O$, $Cd(NO_3)_2 \cdot 4H_2O$ and $Mn(C_2H_3O_2)_2 \cdot 4H_2O$ as the starting materials. Citric acid and ethylene glycol were used as gelling agents for the metallic ions in a nitrate solution. After drying in a sand bath for 24 h, the gel obtained was subjected to successive heat treatments at temperatures of 773, 973, and 1073 K, each of 10 h. In order to measure the electrical resistivities of the samples, the powder thus obtained was pelletized with a pressure of 7.2 MPa prior to final sintering at 1173 K for 10 h in flowing oxygen. The Mn^{3+}/Mn^{4+} content of each sample was determined by redox titration analysis and gave an almost constant ratio 0.58:0.42 for all the samples.

The first crystallographic characterization of the phases was performed by X-ray powder diffraction analysis using a Philips X-Pert diffractometer, working with Cu$K\alpha_1$ and Cu$K\alpha_2$ radiation, Soller slits of 0.04 rad and receiver and divergence slits of 1°. Powder diffraction patterns were Rietveld fitted using the GSAS program [14]. The shape of the Bragg peaks was described by a pseudo-Voigt function. The background was modelled using a linear interpolation function. Scanning electron microscopic (SEM) observations were also performed to give an indication of the compound morphology and compactness using a JEOL JSM-6400 instrument.

The cationic disorder effect has been determined by calculating σ^2 and $\langle r_A \rangle$ using standard ionic radii [15] with values 1.216, 1.18 and an extrapolated value of 1.153 Å for La^{3+}, Ca^{2+} and Cd^{2+} ions, respectively. The results indicate that this family of compounds has an almost constant mean ionic radius of $\langle r_A \rangle = 1.20$ Å.

Magnetic and resistance measurements were conducted in a Quantum Design MPMS-7 SQUID magnetometer. The zero-field cooling (ZFC) and field cooling (FC) curves were performed under an applied field of 10 mT. The order temperature, T_C, was determined from the ZFC curves as the temperature where the minimum of the dM/dT derivative occurs. Temperature dependence of magnetization at 1 T applied field and hysteresis loops at 10 K and up to 7 T were also obtained. The resistance and magneto-resistance versus temperature measurements were taken by using a conventional dc four-wire system, with the magnetic field applied parallel to the current.

3. Results and discussion

The morphology of the obtained compounds is shown in the SEM photograph (taken with 6000 times magnification) of Fig. 1. The microstructure reveals uniform and fine grain growth, less than 1 μm size, as expected from the sol–gel fabrication process used to synthesize the samples. The observed agglomeration of such fine grains is also a direct consequence of the fabrication process used.

At room temperature, the diffraction maxima of all the studied compounds were indexed in an orthorhombic space group (*Pnma*) except for the $La_{0.7}Cd_{0.3}MnO_3$ phase that shows the coexistence of rhombohedral ($R\bar{3}c$) (77%) and orthorhombic (*Pnma*) (23%) space groups (see the inset in Fig. 2). For this composition, we have determined a crystallite size by using the Scherrer equation [16] applied to the highest intensity diffraction peak, giving size values of $d \approx 8$ nm for the ($R\bar{3}c$) phase, and $D \approx 30$ nm for the (*Pnma*) one. Refined cell parameters, volume per formula unit, Z parameter, cation radius distribution, σ^2, and mean ionic radii $\langle r_A \rangle$ are shown in Table 1. Due to the smaller ionic radius of Cd^{2+} ion than the Ca^{2+} one, a decrease in the cell volume should be expected as Cd enters into the composition of the samples. However, there is first an increase of that volume, for the $x = 0.1$ composition. On the other hand, cationic disorder continuously increases as the Cd content increases. The fact that increasing cationic disorder leads to a higher volume cell has been previously reported for other ABO_3 perovskite-like compounds [5]. As a consequence, two competing mechanisms as the size of the doping ion and the level of cationic disorder have to be taken into account in order to explain the determined cell volume for each composition.

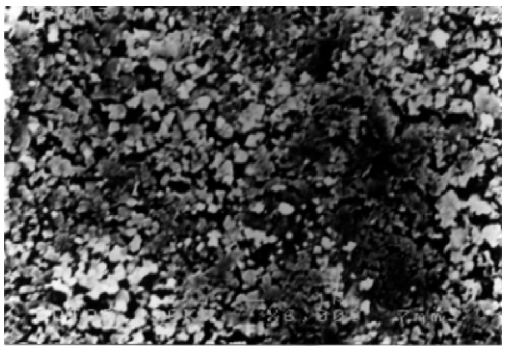

Fig. 1. SEM photograph of the $La_{0.7}Cd_{0.3}MnO_3$ compound sinterized at 900°C.

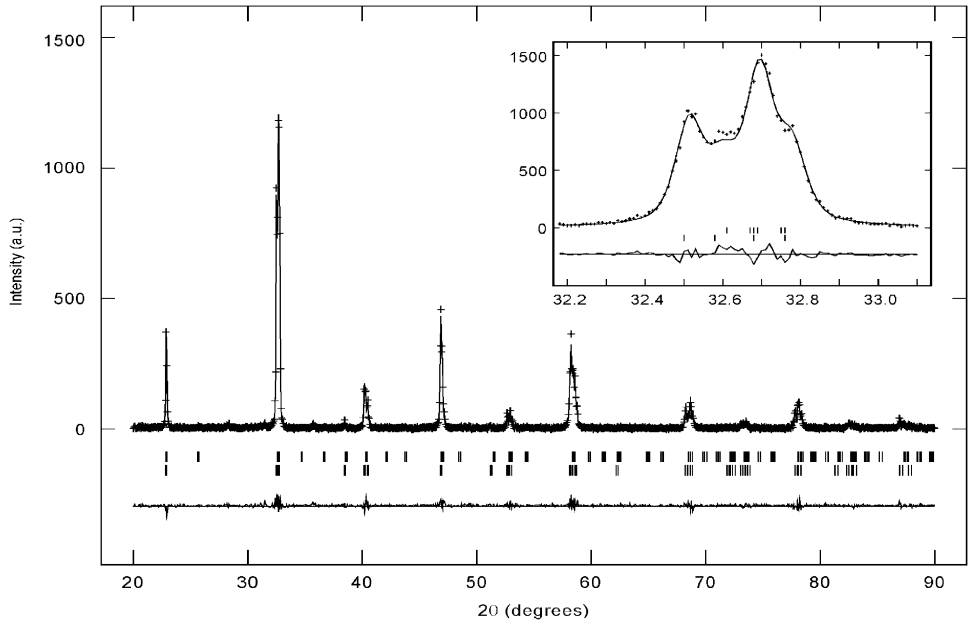

Fig. 2. Rietveld fit to the X-ray powder diffraction data for the $La_{0.7}Cd_{0.3}MnO_3$ compound showing Bragg reflections for both the ($R\bar{3}c$) and *Pnma* phases, difference curve and (inset) refinement of the main diffraction peak, around $2\theta = 32.6°$.

Table 1
Refined cell parameters obtained from the first crystallographic characterization for the $La_{0.7}(Ca_{0.3-x}Cd_x)MnO_3$ ($0 \leqslant x \leqslant 0.3$) family of compounds

Sample	$x = 0$	$x = 0.1$	$x = 0.2$	$x = 0.3$	
Space group	*Pnma*	*Pnma*	*Pnma*	$R\bar{3}c$	*Pnma*
Phase fraction	100%	100%	100%	77%	23%
a (Å)	5.4575(5)	5.4650(2)	5.4616(1)	5.4832(2)	5.4603(7)
b (Å)	7.7057(4)	7.7394(3)	7.7418(2)	—	7.7001(8)
c (Å)	5.4771(4)	5.4795(2)	5.4715(1)	13.3202(5)	5.4678(9)
V (Å^3)	230.34(2)	231.76(3)	231.35(9)	346.82(3)	229.89(4)
Mn–O(1)–Mn (°)	153.8(9)	157.7(1)	157.3(1)	158.5(6)	147.2(8)
Mn–O(2)–Mn (°)	166.5(7)	161.6(3)	161.1(2)		152.5(4)
χ^2	1.987	1.576	1.989	1.63	
R_{wp} (%)	10.26	9.02	9.40	29.77	
R_p (%)	7.78	6.51	6.48	17.21	
Z	4	4	4	6	4
$\langle r_A \rangle$	1.2052	1.2045	1.1997	1.1970	
σ^2	2.72×10^{-4}	4.79×10^{-4}	6.70×10^{-4}	8.46×10^{-4}	

Fig. 3 shows the obtained ZFC–FC curves, for all the compositions. From ZFC curves, we have determined a continuous decrease of the magnetic order or Curie temperature from 270 K for the $Ca_{0.3}$ composition (in good agreement with previous reported data [17,18]) to 90 K for the $Cd_{0.3}$ one. There is a remarkable similarity between the low-field magnetization in samples $x = 0$ and 0.1, indicating that the magnetization process is basically the same: there is a sharp increase in its value around T_C and the measured curves split just below that temperature. The main difference between the $x = 0.2$ and 0.3 compositions is that the irreversibility between ZFC and FC magnetization processes is higher for the latter. However, hysteresis loops (see Fig. 4) show the usual ferromagnetic behaviour for all the Ca-containing samples, quickly reaching magnetic saturation. The low-temperature saturation magnetic moment can be deduced from the Mn^{3+}/Mn^{4+} ratio, which was the same for all the samples, giving a magnetic moment of 3.58 μ_B. The experimental value was determined from Arrott plots [19]. Thus, only the $x = 0$ compound shows the predicted value. The other samples exhibit a continuous decrease in the saturation magnetization. On the other hand, the shape of the measured hysteresis loop together with the sudden decrease of the low-temperature magnetic moment for the fully doped $Cd_{0.3}$

composition (1.59 μ_B) is a clear evidence of strong antiferromagnetic contributions. All measured magnetic data are summarized in Table 2.

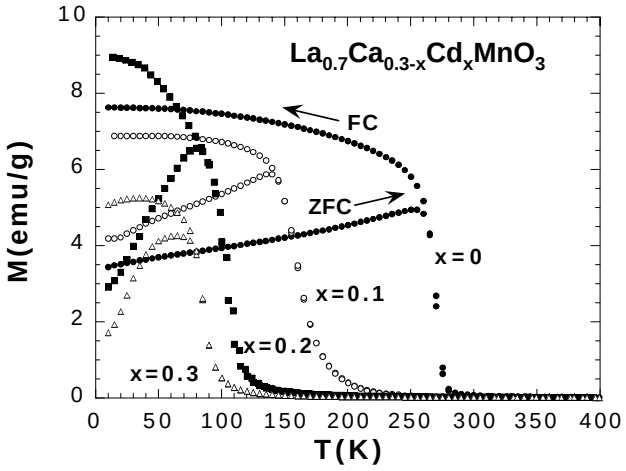

Fig. 3. ZFC (increasing temperature arrow) and FC (decreasing temperature arrow) curves measured for the samples studied in this work.

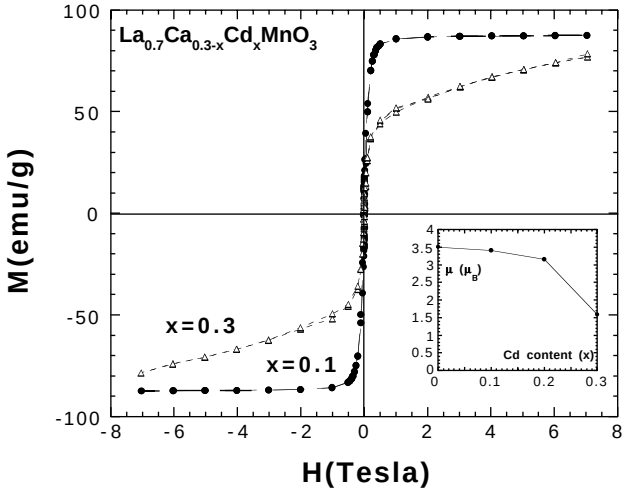

Fig. 4. Hysteresis loops measured at 10 K and up to 7 T, for the $x = 0.1$ and 0.3 compositions. The inset shows the evolution of the measured low-temperature magnetic moment with the Cd content.

To check the ferromagnetic character of all the samples, we can use the temperature dependence of magnetization according to the Bloch's law [20]

$$\frac{M_S(T)}{M_0} = 1 - AT^{3/2}, \quad (1)$$

where M_0 is the saturation magnetization at 0 K and A is a spin wave coefficient that is inversely proportional to the exchange integral, J_{ex}. To summarize already well-known theoretical results, strong ferromagnetic coupling gives rise to high values of the exchange integral J_{ex} and Curie temperature T_C, and low values of A. We have found that the obtained values of A progressively increase as the Cd content in the samples increases. However, we cannot account for the low value of the A coefficient for the fully doped $x = 0.3$ sample, since this composition does not behave as a simple (collinear) ferromagnet, as deduced from the measured hysteresis loop.

The room-temperature measured values of the resistivity range between 0.139 and 0.269 (Ω cm) for the samples with $x = 0$ and 0.3, respectively. When measuring in the absence of applied field, a sharp resistance maximum, characteristic of a semiconductor–metal transition, has been observed for the $x = 0$ and 0.1 compositions, very close to the Curie temperature of those compositions (see Fig. 5). This behaviour is specially marked for the $x = 0.1$ compound and it is a clear indication of an intrinsic (intragrain) mechanism due to the fact that the sample behaves as a granular ferromagnet [1,21].

The $x = 0.2$ and 0.3 samples remain as an insulator down to 80 K where the resistance is too high to be measured within our four-point equipment setup. The values of the ratio $\rho(100\,\mathrm{K})/\rho_0$, where ρ_0 is the resistivity of the sample measured at 300 K and in the absence of applied field, are also shown in Table 2. They clearly indicate the progressive decrease in conductivity as the Cd content increases.

It is already well established that the zero-field resistivity data obtained for $T > T_C$ obey the Mott variable range hopping (VRH) mechanism [22] when the carriers are localized near the Fermi energy, as it is in

Table 2
Values of the order temperature, magnetic moment in the ordered state, magnetization coefficient of the low-temperature spin wave, semiconductor–metallic transition temperature in the resistance behaviour, zero field ratio ρ (100 K)/ρ_0 (where $\rho_0 = \rho$ (300 K)) and calculated energy gap for the $La_{0.7}(Ca_{0.3-x}Cd_x)MnO_3$ ($0 \leqslant x \leqslant 0.3$) family of compounds

x	T_C (K)	μ (μ_B)	A	$T_{SC\text{-}M}$ (K)	ρ (100 K)/ρ_0	ΔE (eV)
0	270	3.50	4.4×10^{-5}	265	0.39	0.164[a]
0.1	165	3.41	8.1×10^{-5}	165	2.1	0.159[a]
0.2	105	3.14	4.4×10^{-4}	70[b]	7.8×10^{3}	3.49[c]
0.3	90	1.59	2.9×10^{-4}	—	1.8×10^{4}	4.39[c]

[a] Data fitted to the polaronic model.
[b] At 6 T applied magnetic field.
[c] Data fitted to the variable range hopping model.

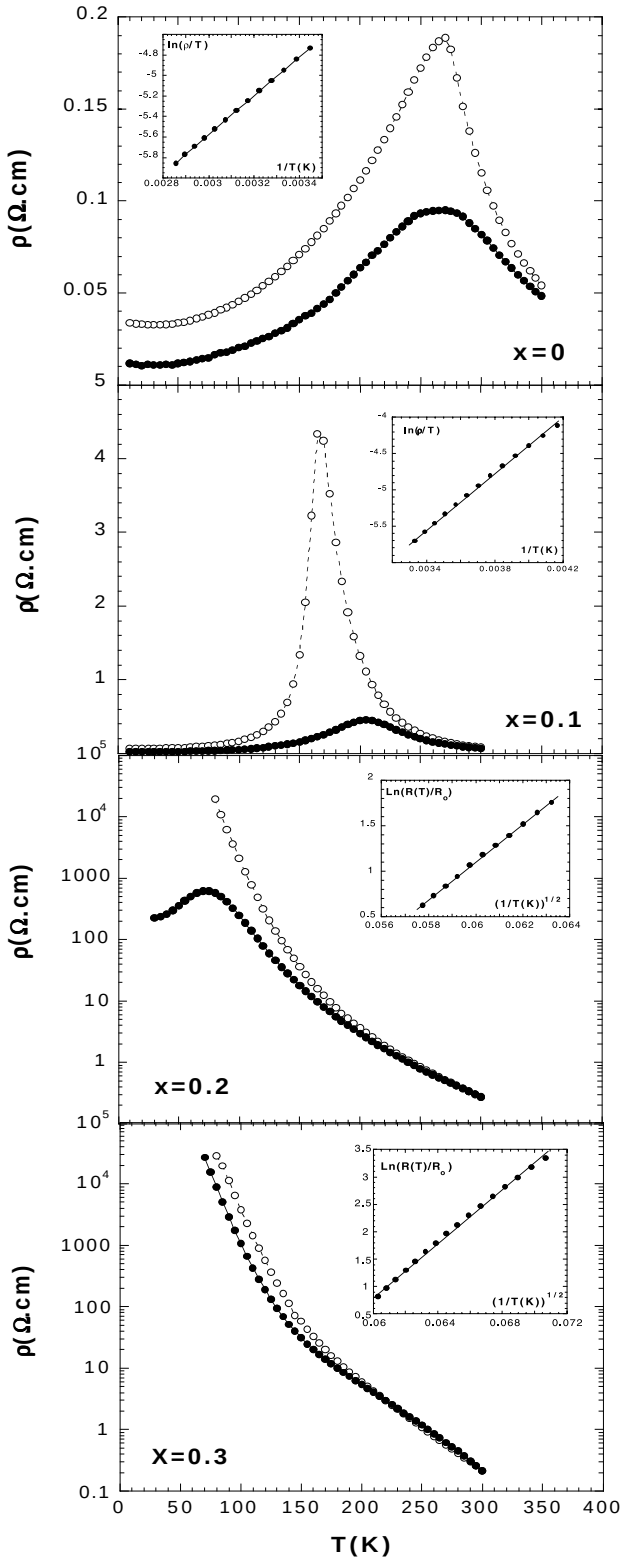

Fig. 5. Temperature dependence of the electrical resistivity for the samples studied in this work. The inset shows the best fit obtained for the high temperature $R(T)$ dependence by using the polaronic model (samples with $x = 0$ and 0.1) or the VRH model (samples with $x = 0.2$ and 0.3).

the case of hole-doped manganites. Previous works [23,24] have determined also that the exponent $n = 1/2$ is the most adequate one for this law. Indeed our zero-field resistance data obey the equation

$$R(T) = R_0 \exp\left(\frac{T_0}{T}\right)^{1/2}. \quad (2)$$

Efros and Shklovii [25] explained that such resistance behaviour is directly related to a form of hopping favoured by the Coulomb repulsion between carriers. Its most important consequence is the existence of an energy or Coulomb gap that basically reflects the differences between the minimum energies of adding an electron and subtracting one from the system, without disturbing the other charges. From the obtained T_0 values, we have estimated values for the Coulomb gap of 2.9 eV for the $La_{0.7}Ca_{0.3}MnO_3$ sample, 4 and 3.49 eV for the $x = 0.1$ and 0.2 compositions, respectively, and 4.4 eV for the $La_{0.7}Cd_{0.3}MnO_3$ one. These values are higher than the energy gaps obtained when $Ln_{0.7}A_{0.3}MnO_3$-type perovskites are synthesized by using the ceramic method [17,26]. We must take care about the fact that our compositions have been synthesized by using the sol–gel method, which gives rise to samples with low grain size, of the order of tenths of nanometers. It is already well established that tunneling of electric charge into small nanoparticles increases the Coulomb energy by the charging effect, strongly enhancing the tunnel resistance. That is, due to the fabrication process used for our compounds, we get samples with higher values of the resistivity and energy gap than the observed ones in manganites fabricated by the ceramic method. This is also justified by the higher value of the electronegativity of Cd (1.69 Pauli) than the Ca one (1 Pauli). As Cd enters into the composition of the samples, strong localization of the charge carriers occurs, leading directly to lower magnetic order temperatures and also to higher energy gap values in the resistance versus temperature behaviour. The determined energy gap values of 3.49 and 4.4 eV for the $x = 0.2$ and 0.3 compositions agree with previous measurements from different authors in other insulating ABO_3 perovskites [27,28]. Nevertheless, for the $x = 0$ and 0.1 compositions, we have got anomalously high values of several eV for the gap energy. In order to elucidate the conduction mechanism in these two compounds, we have also fitted our experimental data to the case of charge carrier mobility of thermally activated form or polaronic model [29]:

$$\ln\left(\frac{\rho}{T}\right) = \ln C + \frac{W}{k_B T} \quad (3)$$

with W as the effective activation energy. For the $La_{0.7}Ca_{0.3}MnO_3$ sample, we obtain now values of the energy gap of 0.164 and 0.159 eV for the $x = 0.1$ composition, which are physically sounder than the

previous obtained ones by using the VRH mechanism. Most probably, both mechanisms are present in the conductive behaviour of all the studied samples, the polaronic mechanism being predominant for the $x = 0$ and 0.1 samples (low content of Cd), while the VHP turns out to be the most important contribution for the $x = 0.2$ and 0.3 compositions (high content of Cd, insulating behaviour).

For $T < T_C$, all samples, except the $x = 0.1$ composition, show intergrain contributions to the resistivity. This electrical conduction mechanism arises from transport of charge carriers between grains. At low temperatures and for small grains, it is increasingly difficult to activate this mechanism. In this situation, transport can be effectively blocked, giving as a result an upturn in the low-temperature resistivity. This effect is the so-called Coulomb blockade [30].

The temperature dependence of the resistance under 6 T applied field has also been measured. It is worth mentioning that the $x = 0.2$ composition shows a field-induced semiconductor–metallic transition, with a transition temperature of 70 K, under 6 T applied magnetic field (see Fig. 5). From those resistance values, we can define the magnetoresistance as $MR(\%) = [1 - R(6\,T)/R(0\,T)] \times 100$. The magnitude of the magnetoresistance change (see Fig. 6) is 49% at 270 K for the $x = 0$ composition and reaches 95% at 165 K for the $x = 0.1$ one. However, the $x = 0.2$ and 0.3 compositions show insulating behaviour in the whole temperature range studied, with values of the magnetoresistance change around the magnetic order temperature of about 85% at 105 K and 74% at 90 K, respectively.

From our experimental results, we can relate the magnetic behaviour of this $La_{0.7}(Ca_{0.3-x}Cd_x)MnO_3$ family of compounds to their structural properties. When the mean radius $\langle r_A \rangle$ remains constant, the systematic change of the magnetic properties can be described by the variation of the metal–insulator transition temperature upon cationic disorder, σ^2. When, as it is in our case, the value of $\langle r_A \rangle$ is low (1.20 Å), that transition temperature and the Curie one are practically in coincidence and this relation may also be applied between σ^2 and T_C [31]. Fig. 7 summarizes the dependence of T_C, σ^2, the magnetization coefficient, B, and the measured low-temperature magnetic moment on the Cd content. In the compositions with only the *Pnma* group (that is, all the Ca-containing samples), there is a linear dependence between these magnitudes and the increase of the cationic disorder, that is the chemical disorder generated in the samples when replacing Ca by Cd ions.

The $La_{0.7}Cd_{0.3}MnO_3$ phase does not follow this behaviour. Although the *Pnma* component has a higher distortion than for the other compositions, the presence of a majority (77%) of less distorted ($R\bar{3}c$) phase could explain the low T_C and the magnetic moment values measured. For this composition, the observed magnetization cluster-like behaviour (see Fig. 3) and the existence of antiferromagnetic interactions (as confirmed by the obtained hysteresis loop, see Fig. 4) hint immediately the idea of phase separation in these compounds. In an intensive review, Dagotto et al. [32]

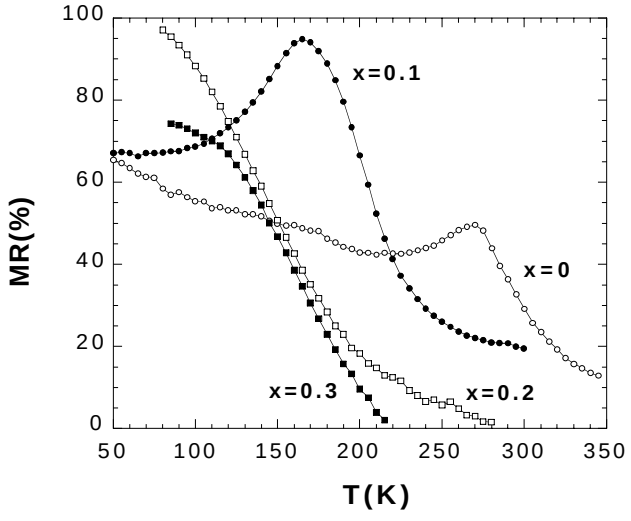

Fig. 6. Magnetoresistance behaviour versus temperature for all the samples studied in this work.

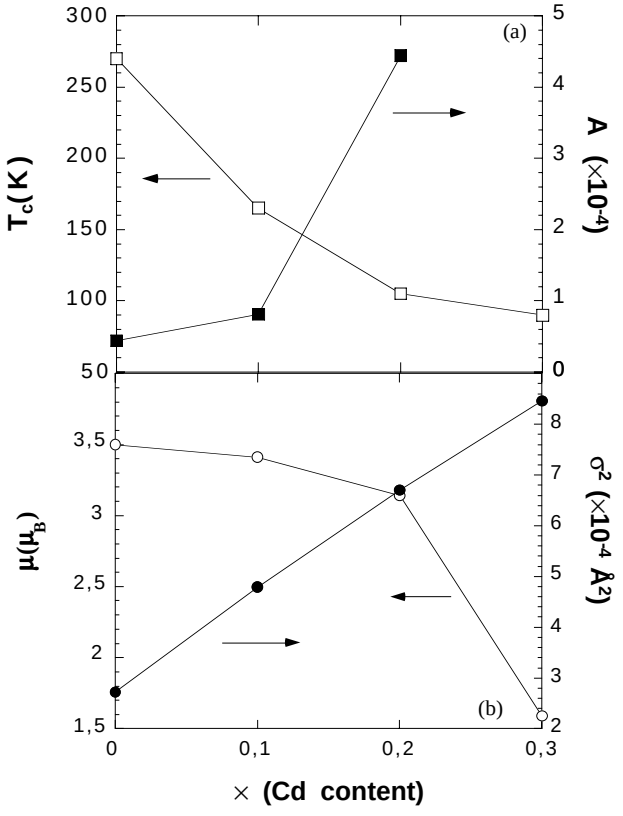

Fig. 7. Dependence on the Cd content in the samples of (a) Curie temperature and low-temperature magnetization coefficient, and (b) low-temperature measured magnetic moment and cationic disorder.

describe both theoretical and experimental work related to the complex spin, charge and/or orbital ordered phases of manganites, in which intrinsic inhomogeneities play a crucial role. The main result is a strong tendency toward phase separation (PS) with the presence of macroscopic ferromagnetic (FM) and antiferromagnetic (AF) regions that, if electronic phase separation between phases is assumed, lead to nanometer-scale coexisting clusters. Due to the existence of two crystallographic phases in the $La_{0.7}Cd_{0.3}MnO_3$ sample, we suggest a model consisting in a matrix of small ($R\bar{3}c$) grains ferromagnetically coupled, and big isolated *Pnma* grains, embedded in that matrix. The two kinds of grains (phases) are of a few nanometers in size and ferromagnetic, but couple antiferromagnetically between them (see Fig. 8). That is, we propose a purely structural phase separation in our studied $La_{0.7}Cd_{0.3}MnO_3$ compound. This picture is similar to the one presented by Okamoto et al. [33] that demonstrated phase separation of two ferromagnetic phases, but with different orbital arrangements.

It has been previously mentioned that the constant Mn^{3+}/Mn^{4+} ratio for all the samples gives an expected value of the low-temperature magnetic moment of $3.58\,\mu_B$, for both phases. Our supposition immediately leads to a low-temperature magnetic moment for such domain configuration of $3.58\,\mu_B \times 0.77$ ($R\bar{3}c$ phase)$-3.58\,\mu_B \times 0.23$ (*Pnma* phase)$= 1.9\,\mu_B$, in rough agreement with the $1.59\,\mu_B$ value experimentally determined. However, there is still another fact that we must consider: the effect of the grain boundaries in such nanometer-sized compounds, which decreases the exchange integral between the ferromagnetically coupled grains of phase ($R\bar{3}c$) [34]. The ferromagnetic exchange at the interface between grains is lower than the ferromagnetic exchange at grain cores, and this effect is stronger as the ratio between boundary and grain size increases. As a direct consequence, the smaller the grain size, the larger the grain boundary influence in the magnetic properties, through the weakening of the exchange interaction. In our case, a ratio between the boundary zone and grain volume of 52% and 8%, for the ($R\bar{3}c$) and *Pnma* phases, respectively, can be easily calculated. That is, the ferromagnetic exchange between grains in the major ($R\bar{3}c$) phase turns out to be reduced due to the grain boundary effect. This fact can account for the small disagreement between the expected ($1.9\,\mu_B$) and measured ($1.59\,\mu_B$) low-temperature magnetic moment value of the $La_{0.7}Cd_{0.3}MnO_3$ compound.

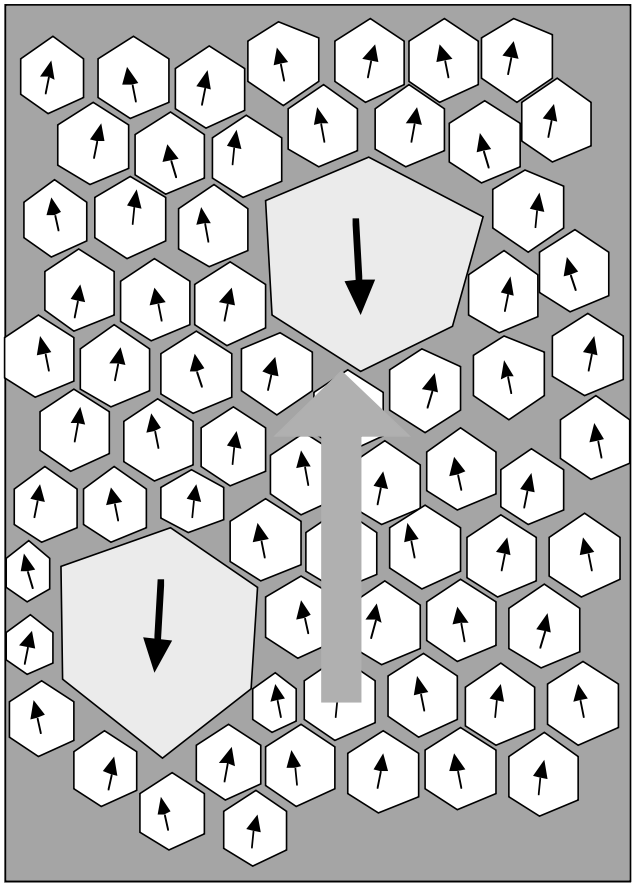

Fig. 8. Schematic representation of the proposed model for the internal structure of the $La_{0.7}Cd_{0.3}MnO_3$ compound.

4. Conclusions

In the light of our experimental work, we can conclude that the main effect of the substitution of Ca by Cd in the classical magnetoresistive $La_{0.7}Ca_{0.3}MnO_3$ composition is a progressive decrease both in the low-temperature spontaneous magnetization and in the Curie temperature value. Despite the constant Mn^{3+}/Mn^{4+} content ratio determined for all the studied compositions, there is evidence that the double exchange is progressively suppressed, weakening the ferromagnetic character and metallic behaviour of the samples. This behaviour can be explained in terms of structural properties in this family of compounds: while for all Ca-containing samples, the main reason arises from the increasing cationic disorder in the composition, for the fully doped Cd one, we propose a phase-separated structure consisting of the coexistence of ferromagnetic grains of a few nanometers size crystallized in different space groups ($R\bar{3}c$, 8 nm size and *Pnma*, 30 nm size, respectively), that couple antiferromagnetically between them. This antiferromagnetic coupling, together with a reduction of the magnetic moment at the grain boundaries of the majority phase, accounts for the low-temperature magnetic moment measured for the $La_{0.7}Cd_{0.3}MnO_3$ compound. This family of samples shows magnetoresistive behaviour, with semiconductor–metallic transition temperatures that decrease as the Cd content increases, except for the fully Cd-doped one,

which shows insulating behaviour in the whole range of temperatures studied.

Acknowledgments

We wish to thank Dr. J.S. Garitaonandia for helpul discussions. We also wish to thank Prof. J.M. San Juan and the Servicio de Microscopía Electrónica de la UPV/EHU. This work has been carried out under project MAT2001-0064 of the Spanish Ministerio de Ciencia y Tecnología.

References

[1] S. Jin, T.H. Tiefel, M. McCormack, R.A. Fastnacht, R. Ramesh, L.H. Chen, Science 264 (1994) 413.
[2] Y. Tokura (Ed.), Colossal Magnetoresistive Oxides, Gordon and Breach Science Publishers, London, New York, 2000.
[3] C. Zener, Phys. Rev. 82 (1951) 403.
[4] K. Chahara, T. Ohno, M. Kasai, K. Kozono, Appl. Phys. Lett. 63 (1993) 1990.
[5] L.M. Rodríguez-Martínez, J.P. Attfield, Phys. Rev. B 54 (1996) R15622.
[6] P.G. Radaelli, D.E. Cox, M. Marezio, S.-W. Cheong, P.E. Schiffer, A.P. Ramirez, Phys. Rev. Lett. 75 (1995) 4488.
[7] J. Alonso, E. Herrero, J.M. González-Calbet, M. Vallet-Regí, J.L. Martínez, J.M. Rojo, A. Hernando, Phys. Rev. B 62 (2000) 11328.
[8] K.A. Thomas, P.S.I.P.N. de Silva, L.F. Cohen, A. Hossain, M. Rajeswari, T. Venkatesan, R. Hiskes, J.L. MacManus-Driscoll, J. Appl. Phys. 84 (1998) 3939.
[9] M. Sahana, M.S. Hegde, N.Y. Vasanthacharya, V. Prasad, S.V. Subramanyam, Appl. Phys. Lett. 71 (1997) 2701.
[10] I.O. Troyanchuk, D.D. Khalyavin, H. Szymczak, Phys. Stat. Sol. (a) 164 (1997) 821.
[11] I.O. Troyanchuk, D.D. Khalyavin, S.N. Pastushonok, J. Phys.: Condens. Matter 10 (1998) 185.
[12] J.P. Araujo, V.S. Amaral, P.B. Tavares, F. Lencart-Silva, A.A.C.S. Lourenço, E. Alves, J.B. Sousa, J.M. Vieira, J. Magn. Magn. Mater. 226–230 (2001) 797.
[13] N.N. Greenwood, A. Earnshaw, in: Chemistry of the Elements, 2nd Edition, Butterworth-Heinemann, Oxford, 1997.
[14] A.C. Larson, R.B. von Dreeler, General Structure Analysis System, Los Alamos National Laboratory, Los Alamos, NM, 1994.
[15] R.D. Shannon, Acta Crystallogr. A32 (1976) 751.
[16] H.P. Klug, L.A. Alexander, X-ray Diffraction Procedures for Polycrystalline and Amorphous Materials, Wiley, New York, 1974.
[17] R. Mahendiran, R. Mahesh, A.K. Raychaudhuri, C.N.R. Rao, Solid State Commun. 94 (1995) 515.
[18] L. Righi, P. Gorria, M. Insausti, J. Gutiérrez, J.M. Barandiarán, J. Appl. Phys. 81 (1997) 5767.
[19] A. Arrott, Phys. Rev. 108 (6) (1957) 1394.
[20] C. Kittel, in: Introduction to Solid State Physics, 7th Edition, Wiley, New York, 1996.
[21] R. von Helmollt, Phys. Rev. Lett. A 54 (1975) 225.
[22] N.F. Mott, J. Non Cryst. Solids 1 (1968) 1.
[23] J. Gutiérrez, A. Peña, J.M. Barandiarán, J.L. Pizarro, L. Lezama, M. Insausti, T. Rojo, J. Phys.: Condens. Matter 12 (2000) 10523.
[24] H. Huhtinen, R. Laiho, K.G. Lisunov, V.N. Stamov, V.S. Zakhvalinskii, J. Magn. Magn. Mater. 238 (2002) 160.
[25] A.L. Efros, B.L. Shklovskii, J. Phys. C: Solid State Phys. 8 (1975) L49.
[26] H. Song, W.J. Kim, S.-J. Kwon, J. Magn. Magn. Mater. 213 (2000) 126.
[27] J.H. Park, C.T. Chen, S.W. Cheong, W. Bao, G. Meigs, V. Chakarian, Y.U. Idzerda, Phys. Rev. Lett. 76 (1996) 4215.
[28] D.S. Dessau, Z.X. Shen, in: Y. Tokura (Ed.), Colossal Magnetoresistive Oxides, Gordon and Breach Science Publishers, London, New York, 2000.
[29] G.J. Snyder, R. Hiskes, S. Dicarolis, M.R. Beasley, T.H. Geballe, Phys. Rev. B 53 (1996) 14434.
[30] M. García-Hernández, F. Guinea, A. de Andrés, J.L. Martínez, C. Prieto, L. Vázquez, Phys. Rev. B 61 (2000) 9549.
[31] L.M. Rodríguez-Martínez, The effect of cation disorder in manganese oxide perovskites, Ph.D. Report, University of Cambridge, 1999.
[32] E. Dagotto, T. Hotta, A. Moreo, Phys. Rep. 344 (2001) 1.
[33] S. Okamoto, S. Ishihara, S. Maekawa, Phys. Rev. B 61 (2000) 451.
[34] L. Del Bianco, A. Hernando, E. Bonetti, E. Navarro, Phys. Rev. B 56 (1997) 8894.